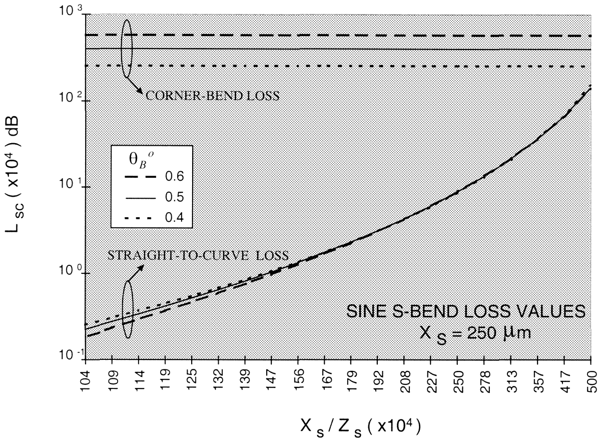

Figure 7 Straight-to-curved transition loss variation as a function of X_s/Z_s for sine S-bends for $X_s = 250$ μm, $\theta_B = 0.4°, 0.5°, 0.6°$, and $\lambda = 1.55$ μm

The loss values have been calculated for a number of assorted values of X_s and Z_s. As can be seen, these loss values are negligibly small. For very low-loss integrated-optic waveguides, such as those reported in [14] with propagation loss values of 0.02 dB/cm, such loss improvements can be meaningful.

IV. CONCLUSION

The new slope-matched sine/cosine S-bend designs presented here show a performance better than that of the conventional sine/cosine S-bends when used for connecting offset straight waveguides inclined with respect to each other; the performance remains better for a wide range of longitudinal and transverse offset parameters. The loss performance of the slope-matched designs can be improved further by incorporating lateral offset between the straight and the curved waveguides.

ACKNOWLEDGMENT

The authors are grateful to Mr. Manu Sharma for some of the calculations, and Mr. Uma Shanker for assistance in drawing some of the figures. Finally, one of the authors (A. M. S.) expresses his sincere appreciation to his parents for their patience and co-operation during the year of this work.

TABLE 2 Calculated Values of Optimum Lateral Offset a_{opt} and the Values of Straight-to-Curve Transition Loss, with and without Lateral Offset, for Cosine S-Bends; $\theta_B = 0.5°$, $x_B = 10$ μm, $z_B = 1146$ μm, and $\lambda = 1.55$ μm

X_s, Z_s (μm)	L_{sc} (Without Offset) (dB)	a_{opt} (μm)	$L_{sc}(a_{opt})$ (With Offset) (dB)
125, 12,000	5.3*e*-05	0.02	2.9*e*-10
125, 9000	3.0*e*-04	0.04	1.0*e*-08
125, 4500	1.4*e*-02	0.29	2.3*e*-05
125, 4000	2.8*e*-02	0.42	9.0*e*-05
125, 3000	1.7*e*-01	1.0	3.2*e*-03
125, 2500	5.8*e*-01	1.9	4.0*e*-02
250, 24,000	1.2*e*-05	8.5*e*-03	7.5*e*-12
250, 18,000	5.9*e*-05	0.15	3.7*e*-10
250, 9000	1.9*e*-03	0.31	4.5*e*-07
250, 8000	3.6*e*-03	0.49	1.5*e*-06

REFERENCES

1. H.F. Taylor, Power loss at directional changes in dielectric waveguides, Appl Opt 13 (1974), 642–647.
2. D. Marcuse, Length optimization of an S-shaped transition between offset optical waveguides, Appl Opt 17 (1978), 763–768.
3. L.D. Hutcheson, I.A. White, and J.J. Burke, Comparison of bending losses in integrated optical circuits, Opt Lett 5 (1980), 276–278.
4. L.M. Johnson and F.J. Leonberger, Low-loss LiNbO$_3$ waveguide bends with coherent coupling, Opt Lett 8 (1983), 111–113.
5. V. Ramaswamy and M.D. Divino, Low-loss bends for integrated optics, Proc Conf Lasers and Electroopt, Washington, DC, 1981, paper THP1.
6. W.J. Minford, S.K. Korotky, and R.C. Alferness, Low-loss Ti:LiNbO$_3$ bends at $\lambda = 1.3$ μm, IEEE J Quantum Electron QE-18 (1982), 1802–1806.
7. R. Baets and P.E. Lagasse, Loss calculation and design of arbitrarily curved integrated-optic waveguides, J Opt Soc Amer 73 (1983), 177–182.
8. F.J. Mustieles, E. Ballesteros, and P. Baquero, Theoretical S-bend profile for optimization of optical waveguide radiation losses, IEEE Photon Technol Lett 5 (1993), 551–553.
9. F. Ladouceur and P. Labeye, A new general approach to optical waveguide path design, J Lightwave Technol 13 (1995), 481–492.
10. T. Kitoh, N. Takato, M. Yasu, and M. Kawachi, Bending loss reduction in silica-based waveguides by using lateral offsets, J Lightwave Technol 13 (1995), 555–562.
11. C. Seo and J.C. Chen, Low transition losses in bent rib waveguides, J Lightwave Technol 14 (1996), 2255–2259.
12. D. Marcuse, Light transmission optics, Van Nostrand Reinhold, New York, 1973.
13. V. Subramaniam, G.N. De Brabonder, D.H. Naghski and J.T. Boyd, Measurement of mode field profiles and bending and transition losses in curved optical channel waveguides, J Lightwave Technol 15 (1997), 990–997.
14. K. Grosskopf, N. Fabricius, and B. Wolf, Fabrication and performance of planar optical couplers in glass for broadband telecommunications networks, Int China Fibercom'94, Shanghai, P. R. China, May 1994, pp. 128–136.

DESIGN OF THE SMART OPTOELECTRONIC NOT GATE BASED ON DIRECTIONAL COUPLERS

Wen-Ching Chang,[1] Yang-Han Lee,[1] Jiang-Duh Fang,[1] Ming-Yung Hsuan,[1] and Li-Ying Chang[1]
[1] Department of Electrical Engineering
Tamkang University
Tamsui, Taipei Hsien, Taiwan 25137, R.O.C.

Received 12 July 1999

ABSTRACT: *A novel smart optoelectronic NOT gate has been proposed. It takes advantage of the linear device operation and the easy-to-implement logic function as compared to conventional optoelectronic logic gates. Detailed investigations of the configuration of the NOT gate, optoelectronic converters, and numerical analysis have been considered.* © 2000 John Wiley & Sons, Inc. Microwave Opt Technol Lett 24: 271–275, 2000.

Key words: *optoelectronic; optical waveguide; logic gate; directional coupler*

I. INTRODUCTION

Optical communication systems have attracted many researchers and have stimulated great developments in high-speed optoelectronic logic gates in recent years. Ultrafast optoelectronic logic gates also will be indispensable in optical communication systems in the near future. Generally, the most commonly used techniques for optoelectronic logic gates were nonlinear optical devices. Although nonlinear operations have been implemented by several methods, these methods still present some difficulties for practical applications.

Following the self-pumped phase conjugate mirror (SPPCM) technique, much research that focused on all-optical logic operations in photorefractive materials such as $BaTiO_3$ crystals has been successfully completed [1–4]. Qiu et al. demonstrated OR, NOT, and NOR optical logic gates by using the induced and erasable SPPCM in photorefractive materials [2].

To our knowledge, bistable devices can be employed as logic gates or flip-flops [5, pp. 546–563]. The bistable device adopted in optoelectronic switching is called the self-electro-optic effect device (SEED). In practical circuit design, we can employ a SEED accompanied by an electronic or electro-optic device to construct a feedback loop. For instance, a SEED can be connected in series with a resistor (R-SEED), with a field-effect transistor (F-SEED), with a heterostructure phototransistor (H-SEED), or with another SEED (symmetric SEED or S-SEED). For most logical operations, multiple SEEDs can be integrated together, and are called logic-SEED (L-SEED). In [6], Ohno et al. implemented a new optical inverter, which is composed of two resonant tunneling transistors, and the logic function is realized by using the monostable–bistable transition of the logic gate. Finally, Hall and Rauschenbach first demonstrated AND and NOT functionalities with a clock stream and a data stream as the logic inputs to an SOA-based switch for the ultrafast nonlinear interferometer [7].

In summary, the key problem of the traditional optoelectronic logic gates is the limitation in nonlinear operation. As a result, it is difficult for practical application in optical computing systems. Hence, the best way to improve the nonlinear operation is to employ devices with a linear function, such as Ti: $LiNbO_3$ directional coupler switches.

This paper is organized as follows. Section II describes the configuration of the smart optoelectronic NOT gate. Section III shows the most essential part of the smart optoelectronic logic, i.e., the directional coupler, describing its architecture and characteristics. Section IV depicts the characteristics of the different optoelectronic (OE) converters. Section V illustrates the characteristics of the directional couplers, such as the switching voltage, device parameters, and crosstalk by means of numerical analysis, and discusses the smart optoelectronic NOT gate. Finally, Section VII is the conclusion.

II. SMART OPTOELECTRONIC NOT GATE CONFIGUATIONS

The smart optoelectronic NOT gate uses electro-optic switches to realize a logic algorithm. The major configurations are composed of directional coupler switches, optoelectronic converters, EDFAs, 1:1 optical couplers, and delay lines. The directional couplers and optoelectronic converters are illustrated in the third and fourth section, respectively. The EDFAs are used to achieve identical input of the power level. In addition, the purpose of the delay lines is to synchronize the optical and electrical signal in the directional coupler.

The circuit configuration and truth table of the smart optoelectronic NOT gate are clearly described as follows. The inverting theorem is implemented by the NOT gate in a 1×1 configuration, as shown in Figure 1(a). The NOT operation is that input A is a complement of output X. In other words, if $A = 1$, then $X = 0$; or if $A = 0$, then $X = 1$, as described in the truth table of Figure 1(b).

III. DIRECTIONAL COUPLER

The most commonly used materials in integrated optical devices can be categorized into three kinds: glass waveguide, III–V compound semiconductors such as GaAs and InP, and isolated ferroelectric crystals such as $LiNbO_3$ and $LiTaO_3$. Among those materials, $LiNbO_3$ has good characteristics of electro-optic (EO) and acousto-optic (AO) modulation.

A. Architecture of Directional Couplers. Because $LiNbO_3$ has many advantages, such as low waveguide loss and high electro-optic coefficients, it is one of the most important materials in integrated optical devices. Among $LiNbO_3$ waveguide devices, titanium-indiffused $LiNbO_3$ (Ti: $LiNbO_3$) is the most mature and well-developed technology. Therefore, a Ti: $LiNbO_3$ directional coupler is a good choice for the design of smart photonic logic gates. The method to implement a directional coupler for *z*-cut Ti: $LiNbO_3$ is described as follows [8]. First, a directional coupler with uniform coupling is designed and fabricated, and the switching voltage is increased due to the coupling constant weighting effect. The second method is employed by the uniform $\Delta\beta$ driving technique, presenting a cross state under the condition of no bias. In the third, selecting titanium thickness controls the polarization state. In the final technique, the electrodes for alternating $\Delta\beta$ were placed on the waveguides [9]; its advantage is to reduce loss and crosstalk. A pair of electrode architectures with a special design is called the COBRA (commuter optique binaire rapide) [10]. In general, the directional coupler with two pairs of electrodes using the alternating $\Delta\beta$ technique is called reversed $\Delta\beta$ [11, 12].

Figure 2(a) is a 2×2 *z*-cut Ti: $LiNbO_3$ directional coupler. Because the architecture is symmetric, there is no difference in the optical path. As we know, it is very important to maintain the synchronization and obtain zero optical path difference in the layout of these smart optoelectronic NOT gates. However, in the actual application and design, the problem of optical path differences should be considered. Hence, the key problem with the polarization rotation of the optical mode can be easily solved. In addition, the electro-optic effect would be influenced by the electric field distribution in the $LiNbO_3$ waveguide, so it is also important to arrange the electrode and choose the crystal orientation. Figure 2(b) shows the arrangement of the electrode and waveguide. Several important parameters of the directional coupler, such as the switching voltage (V_π), the coupling coefficient (κ), the electrode gap (G), and the interaction length (L_c), should be discussed. The analysis of these device parameters will be described in Section V.

B. Analysis of Directional Couplers. The directional coupler is the most essential part of the smart optoelectronic NOT gate. Thus, analysis of the directional coupler is very important. The analysis of the focal point includes low driving voltages,

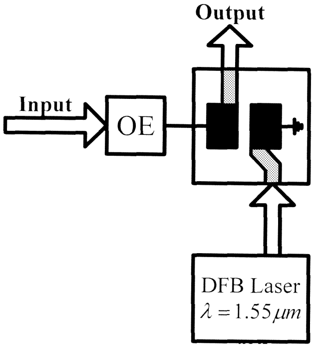

(a)

Input A	Output X
0	1
⬚1	0

(b)

Figure 1 Proposed smart photonic logic NOT gate. (a) Circuit configuration composed of an integrated optical directional coupler and an optoelectronic device. (b) Truth table. Note that the dashed box corresponds to the applied voltage on the directional coupler

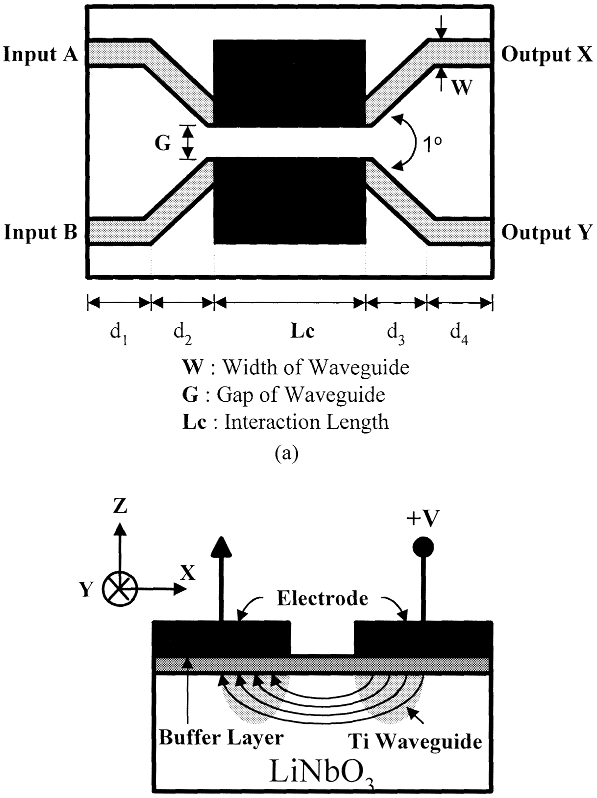

(b)

Figure 2 architecture of 2 × 2 directional coupler. (a) Top view. (b) Cross-section

ultra-high switching frequency, low loss, and low crosstalk. It is expected that the driving voltage of the electro-optic switches is less than 5 V [13]. In [5, pp. 541–543], the switching voltage is considered in the configuration of a COBRA. If $\delta = \sqrt{3}\,\kappa$, then the condition of the switch is in the bar state. The required switching voltage is

$$V_\pi = \frac{\sqrt{3}\,\lambda}{2\gamma L_c} \tag{1}$$

and

$$\gamma = \frac{rn^3}{G}, \; L_c = \frac{\pi}{2\kappa}$$

where λ is the wavelength of laser light, r is the electro-optic coefficient, n is the refractive index, G is the gap, κ is the coupling coefficient, L_c is the interaction length, and γ is an effective parameter representing the effect of electro-optic modulation. Nevertheless, the refractive index is relative to the laser wavelength with a TE and TM mode. For example, at a wavelength of $\lambda = 1.55$ μm, if $\kappa = 0.71 \times 10^{-3}$ 1/m, then $L_c = 2.21$ mm can be determined. If $G = 1$ μm, $r_{33} = 30.8 \times 10^{-12}$ m/V, and $n_{\text{TM}} = 2.144$, we can obtain $\gamma_{\text{TM}} = 3.04 \times 10^{-4}$ 1/V and $V\pi = 2$ V.

IV. OPTOELECTRONIC CONVERTERS

The basic principle of the optoelectronic converter is that a photodiode is used to absorb photons and generate a strong electric field to excite more electron–hole pairs, resulting in a larger photocurrent. These characteristics are satisfied with the smart optoelectronic NOT gate. To match the directional coupler, the optoelectronic converter must include an impedance-matching circuit. If the output voltage is small, a FET amplifier must be used to increase the voltage. Furthermore, optoelectronic converters have many types. These optoelectronic converters based on GaAs, InGaAs, and InGaAsP have been studied and developed. We will introduce six optoelectronic converters as follows.

A. P-I-N PD (P-Type, Intrinsic, N-Type Photodiode). The *p-i-n* photodetector [5, pp. 182–217, 14] has a sandwiched *p-i-n* semiconductor structure inserting an intrinsic (i) layer between n-type and p-type layers. The n-type absorbs incident photons, and then the photocurrent is generated in the intrinsic layer, and the p-type layers usually have relatively higher doping levels compared to the lightly doped intrinsic layer.

B. UTC PD (Unitraveling-Carrier Photodiode). The UTC PD uses the MOCVD technique in the InP substrate [15–18]. The UTC PD, with an absorption (InGaAs) layer and a carrier-collecting layer (InP), enables us to exploit only photoexcited electrons as active carriers in the *p-i-n* structure, and the velocity overshoot in the InP collecting layer enhances the saturation output.

C. MSM PD (Metal–Semiconductor–Metal Photodiode). The MSM PD is similar to the *p-i-n* PD, but the p-type and n-type semiconductors are replaced by metal contacts. These two metal contacts are interleaved in an interdigitated structure to reduce two-plate capacitance. So, the MSM PD has a lower junction capacitance to cause high sensitivity and speeds [19–22].

D. P-I-N / FET. In general, GaAs and InP (InGaAs and AlGaAs) are good materials for FETs (*p-i-n* diodes). However, the sensitivity of a *p-i-n*/FET only has about 100 MHz for the limited transconductance gain from the FET, and it is not as good as the best hybrid circuits [23, 24].

E. HPT. The heterophototransistor (HPT) [25] has a base (p–InGaAs) and collector (n–InGaAs) function as a photodiode at reverse bias. By adding the emitter (n−InP), it creates an *n-p-n* transistor. Because the switching speed of the transistor is dependent on the charging and discharging speed of the base−emitter capacitor, the speed of a phototransistor is determined by the incident light power, which generates the current to charge the base−emitter capacitor. Therefore, it can be used for high-speed and high-sensitivity communications.

F. P-I-N / HBT. The heterojunction bipolar transistors (HBTs) are very important for the applications of ultra-fast-speed logic for microwave power devices [26]. The HBT technology with the conventional multimedia process has two limitations: First, the device topography presents step heights of larger than 1 μm for limitation in large-scale integration. The second limitation is the impossibility of simultaneously decreasing the base transit time and the base resistance for a tradeoff between the base layer thickness and doping concentration. The planar processes with ion implantation or epitaxial regrowth techniques can improve the device performance, the reliability of the metal connections, and the scale integration. These processes would optimize the HBT performances with a thin intrinsic base for a low base transit time and a thick and highly doped extrinsic base for low base resistance [2].

V. NUMERICAL ANALYSIS OF DIRECTIONAL COUPLER

The determination of the gap (G), the interaction length (L_c), and the coupling coefficient (κ) of the directional coupler is dependent on the operating wavelength (λ), TE or TM modes, switching voltages, switch frequency, and crosstalk.

A. Switching Voltage. From Eq. (1), we can obtain the switching voltage of the directional coupler versus the gap at operating wavelengths (λ) of 1.3 and 1.55 μm. The switching voltage of the TE mode is larger than that of the TM mode. As κ increases, the switching voltage increases. Taking $\kappa = 1.0 \times 10^3$ 1/m and a switching voltage of 10 V as an example, we obtain gaps of 1.34 (1.63) and 3.8 μm (4.56 μm) for TE and TM modes, respectively, under an operating wavelength of 1.55 μm (1.3 μm). Given the same value of G, we can use the TM mode at the lower switching voltage. That is, the TM mode switch is a better choice for considering the lower operating voltage.

B. Electrode Gap. We estimate the required gap and coupling coefficient for switching voltages of 2 and 5 V. As the gap increases, the switching voltage increases. Taking $\kappa = 1.0 \times 10^3$ 1/m and a switching voltage of 2 V as an example, we obtain gaps of 0.26 (0.32) and 0.8 μm (0.9 μm) for TE and TM modes, respectively, under an operating wavelength of 1.55 μm (1.3 μm). For a larger switching voltage of 5 V, the gaps are 0.7 μm (0.8) and 1.9 μm (2.3 μm) for TE and TM modes, respectively, under an operating wavelength of 1.55 μm (1.3 μm). It is found that the required gap for the photonic switch is smaller at a wavelength of 1.55 μm.

C. Dielectric Loss. From Eqs. (2) and (3), we obtain the dielectric and propagation loss versus the operating frequency. As the operating frequency increases, the dielectric and propagation loss increases. For operating frequencies of 20 and 100 GHz, we can calculate total losses of 1.48 and 4 dB/cm, respectively.

D. Crosstalk. From Eq. (1) and without consideration of crosstalk, we can obtain the gap versus the interaction length (L_c) for applied voltages of 2 and 5 V together with different wavelengths of 1.3 and 1.55 μm. Taking an interaction length of 10 mm and an operating wavelength of 1.55 μm, the required gaps are 12.3 and 4.96 μm for switching voltages of 5 and 2 V, respectively, under the TM mode. When the gap width is 4 μm, consider the crosstalk to be −20 dB [10]; we need to increase the interaction length from 2.67 (6.67) to 7.84 mm (19.6 mm) for a switching voltage of 5 V (2 V) and an operating wavelength of 1.3 μm. For an operating wavelength of 1.55 μm, the interaction length is not influenced by the crosstalk, and increases from 3.25 to 8.13 mm as the switching voltage decreases from 5 to 2 V. Therefore, an operating wavelength of 1.55 μm is the better solution when the crosstalk is considered.

VI. CONCLUSIONS

The main components of these optoelectronic NOT gates are the integrated optical directional couplers, optoelectronic converters, erbium-doped fiber amplifiers (EDFAs), 1:1 optical couplers, and delay lines. The characteristics of the optoelectronic NOT gate, such as the switching voltage, device parameters, and crosstalk, have been investigated and proved to be informative. The gap (G), the interaction length (L_c), and the coupling coefficient (κ) of the directional coupler can be determined by the operating wavelength, TE or TM modes, switching voltages, and crosstalk. It has been found that the TM-mode optoelectronic switch with an operating wavelength of 1.55 μm is better for lower power and high-speed switches. Under the condition of a TM mode, $L_c =$ 10 mm, and $\lambda = 1.55$ μm, the required gaps are 12.3 and 4.96 μm for switching voltages of 5 and 2 V, respectively. In the near future, it is believed that this will be of great interest in the design of smart optoelectronic systems.

REFERENCES

1. S.K. Kwong, G.A. Rakuljic, and A. Yariv, Real time image subtraction and exclusive or operation using a self-pumped phase conjugate mirror, Appl Phys Lett 48 (1986), 201−203.
2. Y.S. Qiu, H. Li, T.S. Lu, J. Zhuang, and X.C. Gao, Optical logic operations with self-pumped phase-conjugation output in photorefractive materials, Opt Commun 98 (1993), 29−32.
3. H.F. Yau, H.Y. Lee, and P.J. Wang, Optical image-combiner OR gate and optical AND gate using beam fanning effect in $BaTiO_3$ crystals, Opt Eng 33 (1994), 4033−4036.
4. H.Y. Lee, H.F. Yau, and N.J. Cheng, Incoherent optical XOR logic gate and image subtractor with series self-pumped phase conjugators, Opt Eng 37 (1998), 2156−2161.
5. M.M.-K. Liu, Principles and applications of optical communications, Irwin, Homewood, IL, 1996.
6. Y. Ohno, S. Kishimoto, T. Mizutani, and T. Akeyoshi, Logic gate for optical input using monostable-bistable transition of serially connected resonant tunneling transistors, Electron Lett 34 (1998), 250−251.
7. K.L. Hall and K.A. Rauschenbach, 100-Gbit/s bitwise logic, Opt Lett 23 (1998), 1271−1273.
8. M. Kondo, Y. Ohta, Y. Tanisawa, T. Aoyama, and R. Ishikawa, Low-drive-voltage and low-loss polarization-independent $LiNBO_3$ optical waveguide switches, Electron Lett 23 (1987), 1167−1169.
9. H. Kogelnik and R.V. Schmidt, Switched directional couplers with alternating $\Delta\beta$, IEEE J Quantum Electron QE-12 (1976), 396−401.

10. M. Papuchun, Y. Combemale, X. Mathieu, D.B. Ostrowsky, L. Reiber, A.M. Roy, B. Sejourne, and M. Werner, Electrically switched optical directional coupler: Cobra, Appl Phys Lett 27 (1975), 289–291.
11. R.V. Schmidt and H. Kogelnik, Electro-optically switched coupler with stepped $\Delta\ \beta$ reversal using Ti-diffused $LiNbO_3$ waveguides, Appl Phys Lett 28 (1976), 503–506.
12. H. Okayama, A. Matoba, R. Shibuya, and T. Ishida, Optically biased $LiNbO_3$ $\Delta\beta$ reversal directional coupler switch, Electron Lett 23 (1987), 1145–1147.
13. R.V. Schmidt and P.S. Cross, Efficient optical waveguide switch/amplitude modulator, Opt Lett 2 (1978), 45–47.
14. Y.J. Chiu, S.Z. Zhang, S.B. Fleischer, J.E. Bowers, and U.K. Mishra, GaAs-based, 1.55 μm high speed, high saturation power, low-temperature grown GaAs *pin* photodetector, Electron Lett 34 (1998), 1253–1255.
15. Y. Miyamoto, M. Yoneyama, K. Hagimoto, T. Ishibashi, and N. Shimizu, 40Gbit/s high sensitivity optical receiver with uni-travelling-carrier photodiode acting as decision IC driver, Electron Lett 34 (1998), 214–215.
16. K. Sano, K. Murata, T. Akeyoshi, N. Shimizu, T. Otsuji, M. Yamamoto, T. Ishibashi, and E. Sano, Ultra-fast optoelectronic circuit using resonant tunneling diodes and uni-travelling-carrier photodiode, Electron Lett 34 (1998), 215–217.
17. K. Murata, K. Sano, T. Akeyoshi, N. Shimizu, E. Sano, M. Yamamoto, and T. Ishibashi, Optoelectronic clock recovery circuit using resonant tunneling diode and uni-travelling-carrier photodiode, Electron Lett 34 (1998), 1424–1425.
18. M. Yoneyama, Y. Miyamoto, K. Hagimoto, N. Shimizu, T. Ishibashi, and K. Wakita, 40Gbit/s optical gate using optical modulator driven by uni-travelling carrier photodiode, Electron Lett 34 (1998), 1607–1609.
19. R.G. Decorby, R.I. MacDonald, A.J.P. Hnatiw, D. Boertjes, J.N. McMullin, F. Gouin, and J. Noad, Packaged array of eight MSM photodetectors with uniform 12GHz bandwidth, Electron Lett 34 (1998), 400–401.
20. E. Droge, E.H. Bottcher, D. Bimberg, O. Reimann, and R. Steingruber, 70GHz InGaAs metal-semiconductor-metal photodetectors for polarization-insensitive operation, Electron Lett 34 (1998), 1421–1422.
21. T. Chau, L. Fan, D.T.K. Tong, S. Mathai, M.C. Wu, D.L. Sivco, and A.Y. Cho, Long wavelength velocity-matched distributed photodetectors for RF fibre optic links, Electron Lett 34 (1998), 1422–1424.
22. Th. Engel, E. Droge, G. Unterborsch, E.H. Bottcher, and D. Bimberg, Reactive matching of millimetre-wave photodetectors using coplanar waveguide technology, Electron Lett 34 (1998), 1690–1691.
23. K. Kasahara, J. Hayashi, K. Makita, K. Taguchi, A. Suzuki, H. Nomura, and S. Matushita, Monolithically integrated $In_{0.53}Ga_{0.47}As$-PIN/InP-MISFET photo-receiver, Electron Lett 20 (1984), 314–315.
24. S. Hata, M. Ikeda, T. Amano, G. Motosugi, and K. Kurumada, Planar InGaAs/InP PINFET fabricated by Be ion implantation, Electron Lett 20 (1984), 947–948.
25. J.C. Campbell, C.A. Burrus, A.G. Dentai, and K. Ogawa, Small-area high-speed InP/InGaAs phototransistor, Appl Phys Lett 39 (1981), 820–821.
26. R. Driad, P. Desrousseaux, A.M. Duchenois, F. Alexandre, and P. Launay, Planar InGaP/GaAs HBTs for high speed optoelectronic circuit applications, Electron Lett 33 (1997), 85–86.

ELECTROMAGNETIC WAVE SCATTERING FROM 2-D CYLINDER BY USING THE METHOD OF LINES

Jian-Guo Ma,[1] Tze Keong Chia, Tze Wed Tan,[1] and Kye Yak See[1]
[1] School of Electrical and Electronic Engineering
Nanyang Technological University
Singapore 639798

Received 31 August 1999

ABSTRACT: *The method of lines is used to solve electromagnetic wave scattering from a cylinder with arbitrary shapes. The computational efficiency and accuracy are much better than finite difference method and finite element method.* © 2000 John Wiley & Sons, Inc. Microwave Opt Technol Lett 24: 275–277, 2000.

Key words: *electromagnetic wave scattering; method of lines; wave propagation*

I. INTRODUCTION

To solve scattering problems, many numerical methods have been employed, such as finite-difference methods (FDM) [1], finite-element methods (FEM) [2, 5, 6], the boundary element method (BEM) [3], the method of moments (MoM), and so on. It has been demonstrated that these numerical methods are very suitable and flexible in solving electromagnetic (EM) wave scattering (see, e.g., [2, 5, 6] and references therein). However, certain difficulties arise in the application of these methods. For example, artificial boundary conditions (ABCs) must be used to truncate the computation domains for FDM and FEM, which will result in truncating errors, and the ABCs must be relatively far from the scatterers. For BEM, no ABCs are needed, but the Green's function has to be used; thus, a special treatment is necessary for the singularities.

The method of lines (MoL) is a semianalytical method, and has been applied to solve many EM problems [7–10]. Instead of using the original MoL in Cartesian coordinates, modified MoLs (MMoLs) in the cylindrical coordinates [8–10] are used to solve the scattering from conducting cylinders without using any ABCs. Also, the MMoL is semianalytical. For validation, the scattering results from circular conducting cylinders using the MMoL are compared with the analytical solutions from the structures.

II. METHOD OF LINES IN CYLINDRICAL COORDINATES (MMOL)

The general 2-D cylindrical structures are shown in Figure 1. The perfectly conducting cylinder has a general shape Γ under an incident electromagnetic plane wave $\mathbf{F}_z = \mathbf{F}_o e^{jkx}$, where $\mathbf{F}$ represents E_z for TE waves and H_z for TM waves, respectively.

The scattering field satisfies the wave equation in the cylindrical coordinates [4]:

$$\left(\frac{\partial^2}{\partial r^2} + \frac{1}{r}\frac{\partial}{\partial r} + \frac{1}{r^2}\frac{\partial^2}{\partial \theta^2} + k^2\right)F(r, \theta) = 0. \qquad (1)$$

Discretizing the whole region in the angular direction with the step $\Delta\theta$ as shown in Figure 1, Eq. (1) becomes a set of coupled ordinary differential equations with respect to the